8-9-2018

Thermal vibration contribution to continuum stress in the elastic regime

Ranganathan Parthasarathy
Tennessee State University

Recommended Citation

Ranganathan Parthasarathy, "Thermal vibration contribution to continuum stress in the elastic regime", Mechanics Research Communications, Volume 92, 2018, Pages 101-106, ISSN 0093-6413, https://doi.org/10.1016/j.mechrescom.2018.08.009.

Mechanics Research Communications. Year	Publication Office: Elsevier UK
Editor-in-Chief: A. Rosato New Jersey Institute of Technology, Newark, New Jersey, USA Anthony.Rosato@njit.edu	

Thermal vibration contribution to continuum stress in the elastic regime

Ranganathan Parthasarathy[1]

[1]*Postdoctoral Researcher, Department of Mathematical Sciences, Box 9616, Tennessee State University, 3500 John A Merritt Blvd, Nashville, Tennessee 37209-1561, USA*

*Corresponding author rparthas@tnstate.edu
Tel.:+1-816-694-2485; fax: +1-615-963-5099

Abstract

Homogeneous deformation of an ordered crystalline solid at finite temperature can cause non-affine transformation of atomic trajectories. In such a case, continuum measures based on affine transformation of trajectories are insufficient to ensure energetic equivalence between the atomic and continuum scales. We use molecular dynamics simulation of fcc aluminum in NVT ensembles to demonstrate that the second moments of atomic positions about equilibrium show increasing deviation from affine behavior with strain and temperature. While the Cauchy-Born rule enforces affine deformation of the crystal in the static sense, second moments have been used to quantify non-affinity in thermal vibrations due to atomic trajectory transformation under macroscopic deformation. The evolution of second moments with applied strain becomes highly non-linear at high temperatures in the tensile regime as a result of the anharmonic potential energy surface of the material. The vibrational entropy is computed using the time-averaged second moments of position from the molecular dynamics simulation. Stress computed using the resulting free energy is significantly lower than the virial stress in the high tensile strain – high temperature regimes.

Keywords: anharmonic potential, free energy, non-affine thermal vibration

1. Introduction

Continuum stress and strain are routinely computed from molecular dynamics simulations in various applications, particularly for validation or calibration of atomistically-based continuum theories [1–8] in hierarchical multiscale modeling and to specify continuum boundary conditions in concurrent multiscale modeling [8–12]. The Cauchy-Born rule, which enforces affine displacements of atomic equilibrium positions with respect to the boundary strain, is accepted to hold for crystalline materials as long as the crystal undergoes homogeneous deformation in the region of study [7,13,14]. Consequently, it has been widely used to link the atomic scale deformation of a system with the continuum scale deformation. However, at finite temperatures, macroscopic deformation of a crystalline solid changes both equilibrium positions and thermal vibration trajectories of individual atoms, both of which contribute to the change in free energy of the solid. Therefore, continuum stress measures developed from atomistic models aiming to satisfy energy equivalence between the two scales should account for both these effects. Molecular dynamics (MD) is popularly used for finite temperature atomic scale simulations and the virial stress is a diagnostic tool of choice [15] to extract continuum stress from MD. It has been analytically demonstrated [16] that the Piola virial stress – first order deformation gradient pair represents the change in free energy of the discrete system only under the condition that the affine transform applies to not only the equilibrium atomic positions, but also their thermal vibration trajectories. However, the thermal vibration trajectories of individual atoms need not necessarily follow the affine transform, especially at high temperatures. For example, it has been numerically demonstrated that thermal fluctuations can cause non-affine displacements even in a homogeneous crystal [17–20]. Various higher order continuum scale approaches including strain-gradient [21–24] and micromorphic [25–30] have been developed to account for the energetic influence of static non-affinity associated with the violation of Cauchy-Born rule in displacements of equilibrium atomic positions. In contrast, comparatively less attention has been devoted to non-affinity associated with thermal fluctuations. This aspect is particularly important in the

computation of continuum stress in MD simulations, and in the development of finite temperature continuum theory.

We aim to unveil the contribution of non-affine thermal vibrations, as a function of macroscopic strain and temperature, to the free energy, and to the continuum stress, of a crystalline solid undergoing homogeneous deformation with respect to atomic equilibrium positions. We do this using the example of MD simulation of fcc aluminum at temperatures ranging from 150 K to 750 K (0.18Tm to 0.88Tm). At each temperature, we (i) study the evolution of second moments of atomic positions under uniaxial strain, (ii) calculate the Helmholtz free energy, (iii) compute stress from the free energy and compare it with the virial stress, and discuss the significance and implications of the numerical results. The paper is organized as follows. In section 2, we describe the procedures used to compute the entropy and free energy for the system, the resulting continuum stress, and the local deformation gradients. In section 3, we outline the steps used for the molecular dynamics simulation. Finally, we present our observations and inferences in section 4 and conclusions in section 5.

2. Measures of stress and deformation

2.1. Continuum stress calculation

The Piola stress, P^{Ψ}, is computed using the derivative of the total Helmholtz free energy, Ψ, with respect to the deformation gradient. At constant temperature representing a canonical ensemble, it can be expressed as follows.

$$P_{ij}^{\Psi} = \frac{1}{V_0}\frac{\partial \Psi}{\partial F_{ij}} = \frac{1}{V_0}\frac{\partial (U - TS)}{\partial F_{ij}} = \frac{1}{V_0}\frac{\partial \langle \phi \rangle}{\partial F_{ij}} - \frac{1}{V_0} T \frac{\partial S}{\partial F_{ij}} \tag{1}$$

Where V_0 is the undeformed volume, U is the total potential energy, $\langle \phi \rangle$ is the time average of the potential energy, F is the deformation gradient applied to the system boundary, T is the absolute temperature, and S is the entropy of the system. The kinetic energy remains constant at constant temperature and does not contribute to the stress. The potential energy is calculated considering all interactions between the atoms of the system; it does not involve interactions of the system atoms with the heat bath of the canonical ensemble.

The virial stress, denoted as σ^{Virial}, is used as a diagnostic tool to compute continuum stress from molecular dynamics simulation. The virial stress was originally proposed by Clausius and Maxwell [31]; it can be derived in a canonical ensemble by using a generator function to provide the desired canonical transformation under deformation [16,32]. The Cauchy form of the virial stress is defined as follows:

$$\sigma_{ij}^{Virial} = -\frac{1}{V}\left\langle \sum_{\alpha} f_i^{\alpha} r_j^{\alpha} \right\rangle - \frac{1}{V}\left\langle \sum_{\alpha} \frac{p_i^{\alpha} p_j^{\alpha}}{m^{\alpha}} \right\rangle \tag{2}$$

Where V is the deformed volume of the system, α is the atom number, $\vec{f}^{\alpha}$ is the force acting on atom α due to its interaction with all other atoms in the system, $\vec{r}^{\alpha}$ is the instantaneous position vector of atom α, $\vec{p}^{\alpha}$ is the instantaneous momentum of atom α, and m^{α} is its mass. The Piola form of the virial stress, denoted as P^{Virial} is the exact energetic conjugate to the macroscopic deformation gradient when the absolute atomic positions follow the deformation gradient [16,33,34]. On the other hand, the Piola stress defined in Eq.(1), is the exact energetic conjugate to the macroscopic deformation gradient when the entropy calculation is accurate.

2.2. Entropy calculation

The entropy of a periodic crystal can be calculated using several different approaches [35–39]. Here, we employ the method by Kong [36] to compute the phonon frequencies directly from MD trajectories and use Schlitter's approach [37] to calculate the entropy. For a pure crystal whose primitive cell consists of a single atom, the Green's functions $G_{ij}(\vec{q})$ in reciprocal space can be written in the form [36]:

$$G_{ij}(\vec{q}) = \frac{1}{N}\sum_{a,b} \beta_{ij}^{ab} e^{-i\vec{q}\cdot\left(\vec{r}^{a} - \vec{r}^{b}\right)} \tag{3}$$

Where N is the number of atoms in the supercell, $\vec{q}$ is the wavevector, $\bar{r}_i^a$ and $\bar{r}_j^b$ are their equilibrium positions obtained as time averages of the instantaneous positions for atoms a and b, and $\beta_{ij}^{ab} = \langle r_i^a r_j^b \rangle - \bar{r}_i^a \bar{r}_j^b$ are the second moments about equilibrium positions for the atomic pair (a, b) with r_i^a , r_j^b being the instantaneous position vectors of atoms a and b. Clearly, the Green's functions in reciprocal space are the forward Fourier transformations of the second moments. Under conditions where every atom is identical in a periodic lattice, Eq. (3) reduces to $G_{ij}(\vec{q}) = \sum_b \beta_{ij}^{0b} e^{-i\vec{q}\cdot\left(\vec{r}^{0} - \vec{r}^{b}\right)}$, where $\beta^{0b} = \frac{1}{N}\sum_{a=1}^{N} \beta_{ij}^{ab}$ is the atomic average of the second moments between an atom and its b^{th} neighbor. In our calculations, the number of k-points chosen in the reciprocal space is same as the number of atoms in the supercell employed for calculation. The entropy was calculated using Schlitter's expression:

$$S = \frac{1}{2} N k_B \sum_{i=1}^{3} \ln\left(1 + \frac{k_B T e^2}{\left(\hbar/2\pi\right)^2} \beta_i^{eig}\right) \tag{1}$$

where β_i^{eig} are the eigenvalues of the second moments, obtained using the inverse Fourier transform on the eigenvalues of $G_{ij}(\vec{q})$ at the origin. For the case of a homogenous crystal of aluminum, we find that the entropy at 0% strain and 300 K calculated using Schlitter's expression [37] (S = 28.3 J/mol.K) is consistent with experimental results [40,41].

2.3. Local deformation gradient calculations

The deformation gradient at the site of each atom was calculated to verify that the equilibrium displacements of all atoms followed the boundary strain. The following sum of

squares error was minimized using the approach and weight functions proposed by Gullet et al. [42]

$$e^m = \sum_{n=1}^{N} \left(\Delta x_i^{mn} - F_{ij}^m \Delta X_j^{mn}\right)\left(\Delta x_i^{mn} - F_{ik}^m \Delta X_k^{mn}\right) w^n \quad (5)$$

Where e^m is the weighted error in position of atom *m*, Δx_i^{mn} is the vector from the mean position of atom m to the mean position of atom n in the deformed configuration, ΔX_j^{mn} is the same vector in the undeformed configuration, F_{ij}^m is the deformation gradient at the site of atom *m*, and w^n are the weight functions used to weight the error contribution for the atomic pair (*m*,*n*). The weight functions are inversely proportional to the distance between atoms *m* and *n*. The cut-off radius proposed by Gullet et al [42] is assigned based on the spread of β_{ij}^{0b} .

2.4. Evaluation of non-affinity due to thermal vibration

Under Cauchy's rule [16,43], the absolute atomic positions follow the deformation gradient i.e. $r_i^a(t) = F_{ij} R_j^a(t)$ where $r_i^a(t)$ is the position of atom *a* in the deformed configuration at time *t* i.e. it is the trajectory of atom *a* in the deformed configuration, $R_j^a(t)$ is the position of atom *a* in the undeformed configuration at time t i.e. it is the trajectory of atom *a* in the undeformed configuration, and F_{ij} is the deformation gradient corresponding to the representative volume or supercell. Based on a modification proposed by Born to Cauchy's rule, the Cauchy-Born rule states that the mean atomic positions or equilibrium positions are affine with respect to the macroscopic deformation gradient i.e. $\bar{r}_i^a = F_{ij} \bar{R}_j^a$ [16,44], where $\bar{r}_i^a = \langle r_i^a(t) \rangle$ and $\bar{R}_j^a = \langle R_j^a \rangle$. The Cauchy-Born rule investigates the affinity of deformation in a static sense. We further investigate the dynamic affinity of deformation by considering the change in second moments about equilibrium positions under the macroscopic deformation. We denote $\beta_{ij}^{ab} = \langle r_i^a(t) r_j^b(t) \rangle - \bar{r}_i^a \bar{r}_j^b$ as the second moments in the deformed configuration and $\mathrm{B}_{kl}^{ab} = \langle R_k^a(t) R_l^b(t) \rangle$ as the second moments in the undeformed configuration. It follows that if Cauchy's rule is satisfied, the second moments in the deformed configuration $\beta_{ij}^{ab,affine}$ should be related to the second moments in the undeformed configuration through the relationship $\beta_{ij}^{ab,affine} = F_{ik} F_{jl} \mathrm{B}_{kl}^{ab}$. We investigate the dynamic non-affinity by comparing $\beta_{ij}^{ab,affine}$ and β_{ij}^{ab} .

3. Numerical Simulations

The MD simulation was performed using the open source classical molecular dynamics simulation code LAMMPS [45] on a periodic supercell made of 10 X 10 X 10 primitive unit cells of face-centered cubic Aluminum using an embedded atom method (EAM) [46] potential and a Nose-Hoover thermostat to maintain temperature. Periodic boundary conditions (PBC) were used in the three Cartesian directions to simulate an infinite crystal. The simulation was performed in the following steps:

1. The dimensions of the supercell under zero-stress conditions were estimated using time-average of a relaxed stress state (P=0) in the NPT ensemble using 0.5×10^6 time-steps with a time period of 1 fs at T = 300 K.
2. Simulations were then performed at temperatures T = 150, 300, 450, 600, and 750 K under uniaxial strains within elastic regime in the NVT ensemble. For each temperature, the zero-strain supercell dimensions were kept the same as obtained at T = 300 K in step 1. In order to simulate quasi-static loading conditions, the supercell boundaries were deformed as per the applied strain, and atomic positions were initialized at affine equilibrium positions. The deformed supercell at each strain-level was relaxed using 0.5×10^6 time-steps with a time period of 1 fs (achieved converged results). Green strain ε_{11} with $\varepsilon_{22} = \varepsilon_{33} = \varepsilon_{12} = \varepsilon_{23} = \varepsilon_{31} = 0$ was applied along the [100] crystallographic direction and the corresponding deformed edge vectors of the simulation box were computed for each axial strain.
3. For simulation at each strain-level, the atomic average $\beta_{ij}^{0b} = \frac{1}{N} \sum_{p=1}^{N} \beta_{ij}^{ab}$ over all the atoms, as well as atomic average positions were computed using an additional 2.0×10^6 time-steps beyond convergence.
4. Each of the relaxed strained system at 300K from step 2 was then quenched to ~0 K in the NVT ensemble and the stiffness tensors, $k_{ij}^{\mathrm{int},ab} = \left(\frac{\partial^2 \phi}{\partial r_j^a \partial r_i^b} \right)\Big|_{r_i^a = \bar{r}_i^a, r_j^b = \bar{r}_j^b}$, were computed at 5 representative atoms which were sufficiently far from the boundaries of the simulation box. Stiffness tensors including self-terms as well as for the 78 nearest neighbor interactions (b = 0 to 78) were computed. The atomic average of the self-term stiffness values are given by $k_{ii}^{00} = \frac{1}{5} \sum_{pp=1}^{5} k_{ii}^{pp}$ (no summation on repeated index *i* is imposed).
5. The virial stress values at each strain were calculated using the LAMMPS "compute stress per atom" command, summed over all atoms, and averaged over an additional 0.5×10^6 time-steps beyond convergence. Under uniaxial strain, the computed Cauchy stress is equivalent to the Piola stress denoted in the subsequent discussion as P^{Virial}.

4. Results and discussion

The free energy surface of a crystalline material at finite temperature is affected by the uniform affine deformation represented by the deformation gradient as well as by local non-affine fluctuations, which may be static or dynamic, affecting equilibrium atomic positions or vibrations, respectively. In this paper, we focus solely on the local effects arising from dynamic non-affinity by restricting our analysis to the elastic regime where all the atoms follow affine displacements. The local deformation gradients at each atom were computed using the procedure described in section 2.3 and verified to match the deformation gradient at the boundary within a specified tolerance.

4.1. Anharmonicity of energy

Fig. 1(a) shows a log-log plot for the variation of the change in potential energy with tensile strain with the coordinates ($\log \langle \phi\text{-}\phi_0 \rangle$, $\log \varepsilon_{11}$) where the origin has been shifted to ε_{11}=1%. ϕ_0 is the potential energy at zero strain (specification of supercell dimension at zero strain is described in step 2 of section 3). It is clear that the slopes of the lines at all temperatures deviate from 2, implying significant anharmonicity. Although the slopes of the potential energy plots are very close to each other, there is a clear trend of increasing anharmonicity with temperature. The potential energy at 750 K shows nonlinearity on the log-log plot. Fig. 1(b) shows a similar plot for the variation of the Helmholtz free energy with tensile strain with the coordinates ($\log \langle \Psi\text{-}\Psi_0 \rangle$, $\log \varepsilon_{11}$) where the origin has been shifted to ε_{11}=5%, and Ψ_0 is the free energy at zero strain. ε_{11}=5% was chosen since the first non-zero value of $\log (\Psi\text{-}\Psi_0)$ occurs at this strain at 600 K. The free energy plots show significant departure from harmonic behavior at 450 K and 600 K: they are no longer linear even on a log-log scale. The logarithm of free energy for tensile strain at 750 K is negative and has not been shown in Fig. 1.

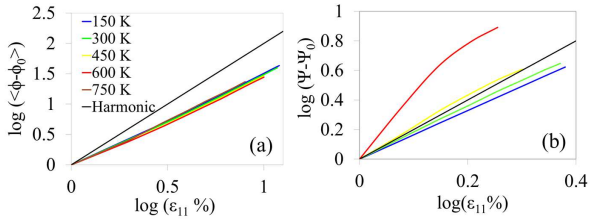

Figure 1 Log-log plot for variation of (a) potential energy and (b) free energy with tensile strain

4.2. Variations in the second moments with loading

Fig. 2(a) shows surface plots for the variation of the atomic average of the self-terms for the second moments of atoms about equilibrium position, $\beta_{ii}^{00} = \frac{1}{N}\sum_{pp=1}^{N} \beta_{ii}^{pp}$ (where N is the number of atoms and no summation on repeated index i is imposed), with applied strain and temperature. The plots compare $\beta_{11}^{00,affine}$ and β_{11}^{00}, described in section 2.4. There is significant discrepancy between the two, with the strongest contrast in the high tensile strain-high temperature regimes. β_{11}^{00} shows non-monotonic behavior in the compressive regime, reaching a minimum at approximately 5% compressive strain at all temperatures.

Fig. 2(b) shows the variation in self-stiffness local force constants, k_{ii}^{00} computed according to step 4 of section 3. We observe a linear decrease in the 11, 22 and 33 components in the tensile regime. As expected from the loading along [100] crystallographic direction, the decrease is anisotropic, and the 22 and 33 components decrease with a smaller slope than the loading direction. The local force constants soften at 5% compressive strain, which corresponds to the minimum value of β_{11}^{00}. We note that affine transformations predict the displacement of atoms purely on a kinematic basis; however non-affine displacements (both static and dynamic) need an energetic basis to explain. Therefore, these observations highlight that the response of the potential energy surface of the material with respect to local fluctuations can be significantly different than its response to affine deformation of all atoms in the crystal.

Fig. 2(c) shows a plot of the second moments at 300, 450, 600, and 750 K normalized with respect to the second moments at 150 K at each value of strain. It is interesting to observe that in the compressive elastic regime, temperature has a nearly linear effect on β_{11}^{00}, which explains why the strain level for minimum β_{11}^{00} is almost invariant with temperature. In the tensile regime, however, higher temperatures amplify the thermal vibrations in a highly non-linear manner, with the amplification showing a rapid increase with increasing tensile strain. The rapidly increasing β_{11}^{00} in the tensile regime can be attributed to the softening of local force constants under tension, particularly the 11 components, as shown in Fig. 2(b). The force constants shown in Fig. 2(b) correspond to zero temperature, and this effect is likely amplified at higher temperatures i.e. the non-linearity increases with both tensile strain and temperature. Furthermore, since we perform uniaxial loading, there is additional tensile stress in the 22 and 33 directions. Similarly, under compression, the increase in the force constants, coupled with the confining effect under uniaxial loading, results in a predominantly linear increase of β_{11}^{00} with temperature, with a much reduced coupled effect of strain and temperature as compared to tension. The results indicate the strong coupled effect of strain and temperature on the local potential surfaces under tension, with consequence on the continuum stress calculations (see section 4.3). For brevity, we do not discuss the variation in inter-atomic second moments and local force constants although they play an important role due to the multibody nature of the EAM potential.

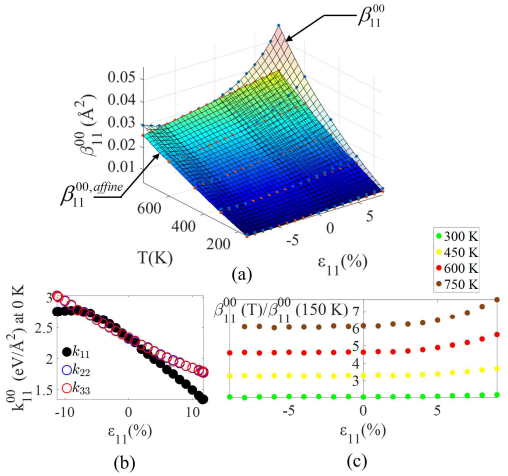

Figure 2 (a) Surface plot for variation of second moments with strain and temperature, compared against prediction from affine transformation, (b) variation of local force constants with applied strain at 0 K, (c) variation of normalized second moments with applied strain.

4.3. Comparison between stress measures

The virial stress including the kinetic contribution in an Eulerian reference frame or spatial description has been accepted as a measure of the Cauchy stress [15,16,32,47]. For the case of uniaxial strain, the Piola stress and the Cauchy stress are equivalent. Therefore, we compare the Piola stress computed per section 2.1 with the virial stress from the MD simulation in Fig. 3. We note that the zero-stress condition at zero-strain only holds for the 300 K simulation. Since the supercell dimensions are kept the same at the other temperatures, there is a non-zero stress at the zero-strain condition. We use that value to shift the stress at zero-strain condition to zero for P^{Ψ} and P^{Virial}. These shift values, which are the thermal stresses at the corresponding temperatures, are shown in Fig. 3(a). The thermal stress values for P^{Ψ} and P^{Virial} are very close at 150 K, and the difference increases with temperature. The reason for the difference is the manner of accounting for the entropic contribution to stress. While the Schlitter's approximation used to compute entropy for P^{Ψ} may somewhat overestimate the entropy at low temperatures [48], at higher temperatures, the affine approximation (intrinsically employed in the virial stress) significantly underestimates the vibrational amplitudes and the resulting entropy change with deformation. Fig. 3(b) shows the stress variation in the compressive loading regime. The differences between P^{Ψ} and P^{Virial} in the compressive regime are almost entirely attributable to the difference in thermal stress at zero strain.

Fig. 3(c) shows the stress variation in the tensile loading regime. The strain value at which P^{Ψ} diverges from P^{Virial} decreases with temperature. Moreover, the percentage difference between P^{Virial} and P^{Ψ} at 9% tensile strain increases from 4% at 300 K to 70% at 750 K. We also note that P^{Ψ} shows a strong qualitative and quantitative resemblance to simulation results from tensile loading of single crystal Aluminum in the [100] direction based on ab-initio molecular dynamics [49]. We attribute the large discrepancy to the entropic contribution to the stress under tensile strain arising from significantly non-affine thermal vibration, which in turn, is a result of the anharmonicity of the potential and free energy surfaces, described in section 4.1. In the context of alloy thermodynamics, vibrational entropy change has been attributed to changes in chemical bond stiffness associated with changes in bond length on the basis of the "bond stiffness vs. bond length" interpretation [50].

The virial stress used to compute P^{Virial} intrinsically incorporates the affine mapping of trajectories, whose efficacy decreases with increasing temperature and strain, as described in section 4.2. As a consequence, the entropic contribution to the stress is underestimated by P^{Virial}. While the entropy computed using the Schlitter's method tends towards an upper estimate of the true value, we emphasize that the entropy contribution in P^{Ψ} has been computed using the second moments directly computed from the MD simulation without any approximation. We therefore postulate that the true stress is likely to lie in between the estimates provided by P^{Ψ} and P^{Virial}. We further explain this result in the framework of higher order continua. The virial stress P^{Virial}, does not automatically incorporate the energetic changes resulting from non-affine local thermal fluctuations. A non-classical continuum theory with a deformation measure representing these local fluctuations would be necessary to capture the effects of changes in local potential wells.

It is highly interesting to observe that P^{Ψ} shows non-linear elasticity and stress-softening behavior at temperatures of 450, 600, and 750 K; the crystal begins to soften at a strain value well within the elastic regime. The softening begins at approximately 8%, 6-8% and 5-6% strain at 450 K, 600 K, and 750 K, respectively. On the other hand, the strain values at which the equilibrium atomic positions violate the Cauchy-Born rule are 11%, 10% and 9% strain at 450, 600, and 750 K, respectively. This stress-softening mechanism is different from the strain-softening shown by P^{Virial} which coincides with the violation of the Cauchy-Born rule, or the appearance of static non-affinity, and is therefore irreversible. The results bear similarities to the experimental observations of Langenecker [51,52], who observed reversible softening of single crystal metals under low amplitude ultrasonic radiation. Softening under uniaxial tension with application of longitudinal ultrasonic vibration has been experimentally observed in several metals and metal alloys [53]. In agreement with the results presented here and in recent work [33], the role of thermal and electronic vibration was found to be profoundly important for deriving equations of state in α-Uranium [54]. Reversible stress-softening under compression has also been reported in soft biological networks including actin networks [55], collagen-based networks [56], and cellulose networks [57], for which entropic contributions are significant even at ambient temperatures.

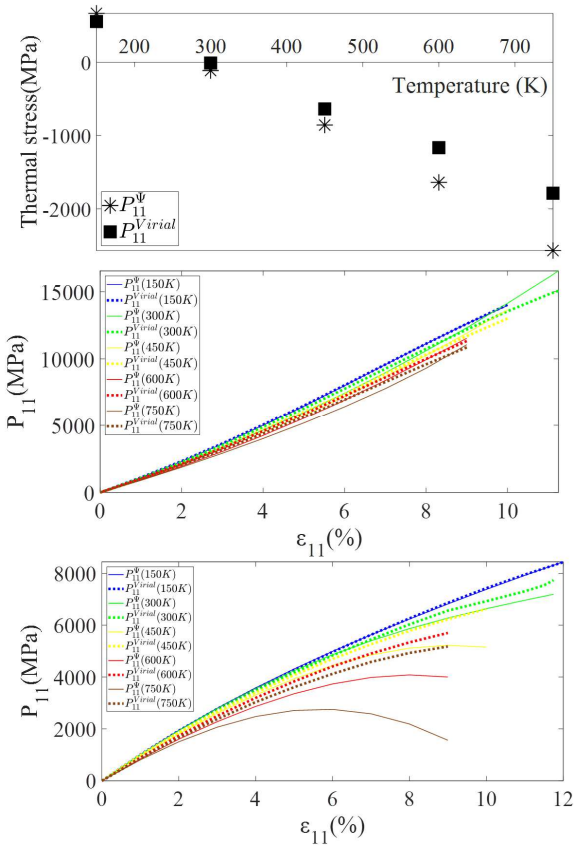

Figure 3 (a) Thermal stress at different temperatures, Piola stress computed using free energy compared with Piola virial stress at T = 150, 300, 450, 600 and 750 K under (b) compressive and (c) tensile strain

5. Conclusion

From the results in this paper, we demonstrate that the anharmonic nature of the interatomic potential becomes important at high temperatures even in the elastic strain regimes where the equilibrium atomic positions follow affine deformation. The importance of higher order elastic coefficients for high temperature events has also been emphasized by Clayton [58]. We have shown that the thermal vibration of atoms, represented by the second moments about equilibrium positions, have a significantly non-linear variation with applied strain and temperature for materials described by anharmonic potentials. This implies that mapping of positions and momenta from deformed to undeformed configurations has complex dependence on strain and temperature. Although higher order virial stresses have been derived for zero-temperature conditions [24], the absence of a higher-order virial stress for finite temperature has been pointed out recently as an open question in nanomechanics [57]. We conjecture here that procedures resembling those developed by Misra [30] or Lemaitre [26] would be suitable to formulate such expressions.

In connecting higher order continuum theories to atomistic descriptions [23,59,60], the effects of macroscopic deformation are only connected to the change in atomic equilibrium positions. However, as we show in this paper, higher order measures of deformation and stress become necessary even when the equilibrium atomic positions of the crystal follow the boundary strain and are completely represented by the first order deformation gradient. Derivation and validation of such measures and the corresponding theories are an active area of research in atomistic-to-continuum multiscale modeling [15,33,61–65].

Our simulations were carried out using the EAM potential on a homogeneous crystal of fcc aluminum for the purpose of demonstrating our ideas, but we expect significant contribution of dynamic non-affinity to the continuum stress for any anharmonic potential. On the other hand, static non-affinity will be significant at small strains and low temperatures for solids with a directional inter-atomic potential [15]. For solids with more complex structure than fcc aluminum, described by directional anharmonic inter-atomic potentials, we expect highly complex evolution of atomic displacements with macroscopic deformation with contribution from both static and dynamic non-affinity, and consequent challenges in the construction of a suitable higher order continuum description. Although our simulations have been carried out for a single crystal metal, the results are strongly likely to be relevant for poly-crystals also due to the presence of preferred orientation in thermo-mechanically processed components [66], particularly with respect to the initiation of dislocations and the onset of plasticity.

In summary, using the example of fcc Aluminum, we have:

(a) Analyzed the highly non-affine and non-linear variation of second moments with strain and temperature, and

(b) Demonstrated the synergistic role of strain and temperature in inducing non-linear elasticity and stress-softening at strain values well within the elastic regime, and at stresses well below the expected yield strength.

Acknowledgements

This research is supported in part by DOE Research Grant DE-NA0002630 (PI: Lizhi Ouyang). The author also acknowledges helpful technical discussion with Dr. Ouyang.

References

[1] M. Arroyo, T. Belytschko, Continuum mechanics modeling and simulation of carbon nanotubes, Meccanica. 40 (2005) 455–469.

[2] H. Jiang, Y. Huang, K.C. Hwang, A comparison of different interatomic potentials: Radius effect of single wall carbon nanotubes, in: IUTAM Symp. Mech. Behav. Micro-Mechanics Nanostructured Mater., 2007: pp. 121–134.

[3] J. Ghanbari, R. Naghdabadi, Multiscale nonlinear constitutive modeling of carbon nanostructures based on interatomic potentials, Comput. Mater. Contin. 10 (2009) 41.

[4] A. V Raghunathan, N.R. Aluru, An empirical potential based quasicontinuum theory for structural prediction of water, J. Chem. Phys. 131 (2009) 184703.

[5] J. Song, Mechanics of Boron Nitride Nanotubes: A Continuum Theory Based on the Interatomic Potential, University of Illinois at Urbana-Champaign, 2007.

[6] H.Q. Jiang, K.C. Hwang, Y. Huang, Mechanics of carbon nanotubes: a continuum theory based on interatomic potentials, in: Key Eng. Mater., 2007: pp. 11–20.

[7] M. Arroyo, T. Belytschko, An atomistic-based finite deformation membrane for single layer crystalline films, J. Mech. Phys. Solids. 50 (2002) 1941–1977.

[8] F. Cleri, S.R. Phillpot, D. Wolf, S. Yip, Atomistic simulations of materials fracture and the link between atomic and continuum length scales, J. Am. Ceram. Soc. 81 (1998) 501–516.

[9] C. Schäfer, H.M. Urbassek, L. V Zhigilei, B.J. Garrison, Pressure-transmitting boundary conditions for molecular-dynamics simulations, Comput. Mater. Sci. 24 (2002) 421–429.

[10] F. Cleri, Representation of mechanical loads in molecular dynamics simulations, Phys. Rev. B. 65 (2001) 14107.

[11] C.L. Brooks Iii, M. Karplus, Deformable stochastic boundaries in molecular dynamics, J. Chem. Phys. 79 (1983) 6312–6325.

[12] M. Berkowitz, J.A. McCammon, Molecular dynamics with stochastic boundary conditions, Chem. Phys. Lett. 90 (1982) 215–217.

[13] A. Aghaei, M.J.A. Qomi, M.T. Kazemi, A.R. Khoei, Stability and size-dependency of Cauchy--Born hypothesis in three-dimensional applications, Int. J. Solids Struct. 46 (2009) 1925–1936.

[14] P. Steinmann, A. Elizondo, R. Sunyk, Studies of validity of the Cauchy--Born rule by direct comparison of continuum and atomistic modelling, Model. Simul. Mater. Sci. Eng. 15 (2006) S271.

[15] J.A. Zimmerman, R.E. Jones, J.A. Templeton, A material frame approach for evaluating continuum variables in atomistic simulations, J. Comput. Phys. 229 (2010) 2364–2389. doi:10.1016/j.jcp.2009.11.039.

[16] E.B. Tadmor, R.E. Miller, Modeling materials: continuum, atomistic and multiscale techniques, Cambridge University Press, 2011.

[17] S. Ganguly, S. Sengupta, P. Sollich, Statistics of non-affine defect precursors: tailoring defect densities in colloidal crystals using external fields, Soft Matter. 11 (2015) 4517–4526.

[18] A. Mitra, S. Ganguly, S. Sengupta, P. Sollich, Non-affine fluctuations and the statistics of defect precursors in the planar honeycomb lattice, J. Stat. Mech. Theory Exp. 2015 (2015) P06025.

[19] S. Ganguly, S. Sengupta, Excess vibrational modes of a crystal in an external non-affine field, J. Chem. Sci. 129 (2017) 891–897.

[20] S. Ganguly, S. Sengupta, P. Sollich, M. Rao, Nonaffine displacements in crystalline solids in the harmonic limit, Phys. Rev. E. 87 (2013) 42801.

[21] V.E. Tarasov, Lattice model with nearest-neighbor and next-nearest-neighbor interactions for gradient elasticity, Discontinuity,

Nonlinearity Complex. 4 (2015) 11–23. doi:10.5890/DNC.2015.03.002.

[22] G. Rosi, N. Auffray, Anisotropic and dispersive wave propagation within strain-gradient framework, Wave Motion. 63 (2016) 120–134. doi:10.1016/j.wavemoti.2016.01.009.

[23] M. Arndt, M. Griebel, Derivation of Higher Order Gradient Continuum Models from Atomistic Models for Crystalline Solids, Multiscale Model. Simul. 4 (2005) 531–562. doi:10.1137/040608738.

[24] N.C. Admal, J. Marian, G. Po, The atomistic representation of first strain-gradient elastic tensors, J. Mech. Phys. Solids. 99 (2017) 93–115.

[25] A. Zaccone, E. Scossa-Romano, Approximate analytical description of the nonaffine response of amorphous solids, Phys. Rev. B. 83 (2011) 184205.

[26] A. Lemaitre, C. Maloney, Sum rules for the quasi-static and visco-elastic response of disordered solids at zero temperature, J. Stat. Phys. 123 (2006) 415.

[27] A. Misra, P. Poorsolhjouy, Grain- and macro-scale kinematics for granular micromechanics based small deformation micromorphic continuum model, Mech. Res. Commun. 81 (2017) 1–6. doi:10.1016/j.mechrescom.2017.01.006.

[28] A. Misra, P. Poorsolhjouy, Granular micromechanics based micromorphic model predicts frequency band gaps, Contin. Mech. Thermodyn. 28 (2016) 215–234. doi:10.1007/s00161-015-0420-y.

[29] A. Misra, P. Poorsolhjouy, Elastic behavior of 2d grain packing modeled as micromorphic media based on granular micromechanics, J. Eng. Mech. 143 (2016) C4016005.

[30] A. Misra, C.S. Chang, Effective elastic moduli of heterogeneous granular solids, Int. J. Solids Struct. 30 (1993) 2547–2566. doi:10.1016/0020-7683(93)90165-4.

[31] J. Clerk-Maxwell, Van der Waals and the continuity of the Gaseous and Liquid state, Nature. 10 (1874) 477–480.

[32] N.C. Admal, E.B. Tadmor, A unified interpretation of stress in molecular systems, J. Elast. 100 (2010) 63–143. doi:10.1007/s10659-010-9249-6.

[33] R. Parthasarathy, A. Misra, L. Ouyang, S. Aryal, L. Ouyang, Finite-temperature stress calculations in atomic models using moments of position, J. Phys. Condens. Matter. 30 (2018) 265901. doi:10.1088/1361-648X/aac52f.

[34] R. Parthasarathy, A. Misra, S. Aryal, L. Ouyang, Phonon Dispersion Evolution in Uniaxially Strained Aluminum Crystal, Contin. Mech. Thermodyn. (2018).

[35] L.T. Kong, G. Bartels, C. Campañá, C. Denniston, M.H. Müser, Implementation of Green's function molecular dynamics: An extension to LAMMPS, Comput. Phys. Commun. 180 (2009) 1004–1010. doi:10.1016/j.cpc.2008.12.035.

[36] L.T. Kong, Phonon dispersion measured directly from molecular dynamics simulations, Comput. Phys. Commun. 182 (2011) 2201–2207. doi:10.1016/j.cpc.2011.04.019.

[37] J.J. Schlitter, Estimation of absolute and relative entropies of macromolecules using the covariance matrix, Chem. Phys. Lett. 215 (1993) 617–621. doi:10.1016/0009-2614(93)89366-P.

[38] H. Schäfer, A.E. Mark, W.F. Van Gunsteren, Absolute entropies from molecular dynamics simulation trajectories Absolute entropies from molecular dynamics simulation trajectories, 7809 (2000). doi:10.1063/1.1309534.

[39] J.H. Weiner, Statistical mechanics of elasticity, Courier Corporation, 2012.

[40] J.D. Cox, D.D. Wagman, V.A. Medvedev, CODATA key values for thermodynamics, Chem/Mats-Sci/E, 1989.

[41] M.W. Chase, NIST—JANAF Thermochemical Tables (Journal of Physical and Chemical Reference Data Monograph No. 9), Am. Inst. Phys. (1998).

[42] P.M. Gullett, M.F. Horstemeyer, M.I. Baskes, H. Fang, A deformation gradient tensor and strain tensors for atomistic simulations, Model. Simul. Mater. Sci. Eng. 16 (2008) 015001. doi:10.1088/0965-0393/16/1/015001.

[43] A.-L. Cauchy, Sur l'équilibre et le mouvement d'un système de points matériels sollicités par des forces d'attraction ou de répulsion mutuelle, Exerc. Mathématiques. 3 (1828) 1827.

[44] M. Born, K. Huang, M. Lax, M.T. Dove, B. Fultz, Introduction to lattice dynamics, Am. J. Phys. 4 (1955) 474. doi:10.1016/j.pmatsci.2009.05.002.

[45] S. Plimpton, Fast Parallel Algorithms for Short-Range Molecular Dynamics, J. Comput. Phys. 117 (1995) 1–19. doi:10.1006/jcph.1995.1039.

[46] M.S. Daw, M.I. Baskes, Embedded-atom method: Derivation and application to impurities, surfaces, and other defects in metals, Phys. Rev. B. 29 (1984) 6443.

[47] A.K. Subramaniyan, C.T. Sun, Continuum interpretation of virial stress in molecular simulations, Int. J. Solids Struct. 45 (2008) 4340–4346. doi:10.1016/j.ijsolstr.2008.03.016.

[48] I. Andricioaei, M. Karplus, On the calculation of entropy from covariance matrices of the atomic fluctuations, J. Chem. Phys. 115 (2001) 6289–6292.

[49] W. Zhou, Y. Zhang, H. Sun, C. Chen, Ideal strength and structural instability of aluminum at finite temperatures, Phys. Rev. B. 86 (2012) 54118.

[50] A. Van De Walle, G. Ceder, The effect of lattice vibrations on substitutional alloy thermodynamics, Rev. Mod. Phys. 74 (2002) 11.

[51] B. Langenecker, Effect of sonic and ultrasonic radiation on safety factors of rockets and missiles, AIAA J. 1 (1963) 80–83.

[52] B. Langenecker, Effects of ultrasound on deformation characteristics of metals, IEEE Trans. Sonics Ultrason. 13 (1966) 1–8.

[53] C. Ye, The effect of ultrasonic waves on tensile behavior of metal, (2016).

[54] M.E. Manley, Vibrational softening in a-uranium, Challenges Plutonium Sci. (2000) 202–207.

[55] O. Chaudhuri, S.H. Parekh, D.A. Fletcher, Reversible stress softening of actin networks, Nature. 445 (2007) 295.

[56] F.G. Torres, O.P. Troncoso, E.R. Rivas, C.G. Gomez, D. Lopez, Reversible stress softening of collagen based networks from the jumbo squid mantle (Dosidicus gigas), Mater. Sci. Eng. C. 37 (2014) 9–13.

[57] F.G. Torres, O.P. Troncoso, D. Lopez, C. Grande, C.M. Gomez, Reversible stress softening and stress recovery of cellulose networks, Soft Matter. 5 (2009) 4185–4190.

[58] J.D. Clayton, Nonlinear mechanics of crystals, Springer Science & Business Media, 2010.

[59] R. Pyrz, B. Bochenek, Discrete-Continuum Transition in Modelling Nanomaterials, in: IUTAM Symp. Model. Nanomater. Nanosyst., 2009: pp. 63–74.

[60] J.A. Zimmerman, D.J. Bammann, H. Gao, Deformation gradients for continuum mechanical analysis of atomistic simulations, Int. J. Solids Struct. 46 (2009) 238–253. doi:10.1016/j.ijsolstr.2008.08.036.

[61] A.M. Krivtsov, V.A. Kuz'kin, Derivation of equations of state for ideal crystals of simple structure, Mech. Solids. 46 (2011) 387.

[62] A.M. Krivtsov, V.A. Kuzkin, Discrete and Continuum Thermomechanics, (2017).

[63] V.A. Kuzkin, A.M. Krivtsov, An analytical description of transient thermal processes in harmonic crystals, Phys. Solid State. 59 (2017) 1051–1062.

[64] A.Y. Panchenko, E.A. Podolskaya, A.M. Krivtsov, Analysis of equations of state and determination of the Grüneisen function for two-dimensional crystal lattices, in: Dokl. Phys., 2017: pp. 141–144.

[65] V.A. Kuzkin, A.M. Krivtsov, R.E. Jones, J.A. Zimmerman, Material frame representation of equivalent stress tensor for discrete solids, Phys. Mesomech. 18 (2015) 13–23.

[66] K.-H. Jung, D.-K. Kim, Y.-T. Im, Y.-S. Lee, Crystal plasticity finite element analysis of texture evolution during rolling of fcc polycrystalline metal, Mater. Trans. 54 (2013) 769–775.